



Hydrothermal synthesis and properties of pigments Chinese purple $\text{BaCuSi}_2\text{O}_6$ and dark blue $\text{BaCu}_2\text{Si}_2\text{O}_7$



Yan Chen, Yuan Zhang, Shouhua Feng*

State Key Laboratory of Inorganic Synthesis and Preparative Chemistry, College of Chemistry, Jilin University, Changchun 130012, People's Republic of China

ARTICLE INFO

Article history:

Received 19 November 2013

Received in revised form

22 January 2014

Accepted 25 January 2014

Available online 14 February 2014

Keywords:

Hydrothermal synthesis

Chinese purple

Near-infrared luminescence

Pigment

Spin gap

Scottyite

ABSTRACT

A green chemistry strategy was developed to prepare two barium copper silicate pigments. Chinese purple $\text{BaCuSi}_2\text{O}_6$ and dark blue $\text{BaCu}_2\text{Si}_2\text{O}_7$ are synthesized through mild hydrothermal treatment in narrow pH range. The compounds are characterized by powder X-ray diffraction techniques, infrared spectroscopy, X-ray photoelectron spectroscopy, energy dispersive spectroscopy, luminance and magnetic measurements. When excited by a visible laser, hydrothermally synthetic $\text{BaCuSi}_2\text{O}_6$ exhibits a broad emission in the near-infrared region with an excited state lifetime 6.4 μs due to the square-planar Cu^{2+} ions as the chromophores. Magnetic analysis of $\text{BaCuSi}_2\text{O}_6$ indicates the spin gapped antiferromagnetic property due to the presence of the Cu–Cu dimers in the structure. $\text{BaCu}_2\text{Si}_2\text{O}_7$ shows interesting quasi-one-dimensional antiferromagnetic property.

© 2014 Elsevier Ltd. All rights reserved.

1. Introduction

Dyes and pigments are the materialized forms of color, which play an important role as information and communication media in human social systems. Due to the shortage of blue and purple inorganic pigments in nature, ancient craftsmen took advantage of their skills and began to manufacture them since 2500 BC [1,2]. The famous man made pigments are the Egyptian blue $\text{CaCuSi}_4\text{O}_{10}$, Chinese blue $\text{BaCuSi}_4\text{O}_{10}$, and Chinese purple $\text{BaCuSi}_2\text{O}_6$ [3–5]. Modern scientific studies of these pigments show that they exhibit the excellent near-infrared (NIR) luminescence properties [6,7]. New interest in these ancient pigments includes their application as advanced functional materials, such as nanomaterials and optical sensors [8,9].

Chinese purple $\text{BaCuSi}_2\text{O}_6$, also termed Han purple, which is well known to museum scientists as the synthetic pigments first produced in ancient China during the period of the Warring States (approx. 1200 BC). Han purple was widely used in the Qin and Han periods. One good example is the paint covering the Terracotta Army found in the tomb of the first Chinese Emperor Qin Shihuan, Xian, China [10]. Chinese purple $\text{BaCuSi}_2\text{O}_6$ has up to now not been detected in natural minerals. Dark blue $\text{BaCu}_2\text{Si}_2\text{O}_7$ is found as a natural mineral,

Scottyite, recently discovered in the Wessels mine, Kalahari Manganese Fields, Northern Cape Province, South Africa [11]. Scottyite, associated with other minerals, appears to have formed as a result of a hydrothermal event. It is, however, found only rarely and only in traces. It is quite hard to be prepared in large scale so far, which hampers the application of the dark blue $\text{BaCu}_2\text{Si}_2\text{O}_7$ as a pigment.

The special chemical and physical properties of Chinese purple are derived from the microscopic structure. The unique colour of Chinese purple is based on the inclusion of square-planar Cu^{2+} ions as chromophores in the environment of a rigid layered framework $\text{Cu}_2(\text{SiO}_3)_4$, which contains an unusual isolated arrangement of $\text{Si}_4\text{O}_{12}^{8-}$ rings and Cu–Cu dimers. When excited in the broad visible spectral window (450–800 nm), Chinese purple was presumed to show an intense and broad emission in the NIR range (800–1200 nm) as similar as Egyptian blue $\text{CaCuSi}_4\text{O}_{10}$ does [3,12]. One hindering feature is the difficulty of the preparation of a suitable sample for characterization. Such broad 800–1200 nm NIR emission of the phosphors are quite useful, which has potential applications in NIR-based biomedical imaging, silica-based optical amplifier, security ink, laser technology and optical sensor [8,13,14]. Furthermore, there are chemically labile Cu–Cu metal bonds in Cu–Cu dimers in $\text{BaCuSi}_2\text{O}_6$, which means that Chinese purple has a low chemical stability and special physical property. The novel spin = 1/2 dimer arrangement makes $\text{BaCuSi}_2\text{O}_6$ a quite interesting compound for physical scientists, related to several important

* Corresponding author.

E-mail addresses: shfeng@mail.jlu.edu.cn, shfeng@jlu.edu.cn (S. Feng).

quantum spin systems [15]. First, $\text{BaCuSi}_2\text{O}_6$ is a spin gapped (SG) antiferromagnet with strong electronic coupling occurs in the Cu–Cu dimers. SG antiferromagnetic (AFM) systems show a quantum spin liquid ground state with a singlet–triplet energy gap. When $\text{BaCuSi}_2\text{O}_6$ sample is applied by a critical magnetic field, the energy of the lowest triplet state ($S_z = +1$, bosons) becomes lower than that of a singlet state ($S = 0$) and a magnetic field-induced Bose–Einstein condensation (BEC) of the excitations occurs. The population of the bosons may be precisely tuned by the applied magnetic field [16]. Second, there is also an interesting dimensional crossover around 1 K from a 3D into a 2D regime with decreasing temperature [17].

$\text{BaCu}_2\text{Si}_2\text{O}_7$ is a quasi-one-dimensional Cu^{2+} ($S = 1/2$) chain compound. A single crystal sample exhibits novel quantum spin = 1/2 chain AFM property with tunable super-exchange interactions [18]. Materials with quasi-one-dimensional magnetic subunits have greatly contributed to the understanding of many-body quantum mechanics. However, magnetic study of $\text{BaCuSi}_2\text{O}_6$ and $\text{BaCu}_2\text{Si}_2\text{O}_7$ based on pure powders were not given yet.

Chinese purple was first synthesized by skilled ancient Chinese craftsmen through solid state reaction. Lead salts were used as flux in the BaO – CuO – SiO_2 system to reduce the reaction temperature (ca. 900 °C) [10]. Chinese purple $\text{BaCuSi}_2\text{O}_6$ will decompose to Chinese blue $\text{BaCuSi}_4\text{O}_{10}$ with Cu_2O and BaSiO_3 when the temperature is higher than 1050 °C, which makes the $\text{BaCuSi}_2\text{O}_6$ quite hard to be prepared through solid state reactions as a pure phase even under laboratory control. For example, well ground mixtures of BaCO_3 , CuO and quartz powders were prepared with stoichiometric ratios 1:1:2 and heated at 900 °C in air for 20 h, then sintered again at 1010 °C in air for 20 h. But $\text{BaCu}_2\text{Si}_2\text{O}_7$, $\text{BaCuSi}_4\text{O}_{10}$, $\text{Ba}_4\text{Si}_6\text{O}_{16}$, BaSiO_3 , and Cu_2O impurities were found in traces (total 7% wt.) [19]. However, the feasible strategy for large-scale preparations of $\text{BaCu}_2\text{Si}_2\text{O}_7$ and $\text{BaCuSi}_2\text{O}_6$ was seldom reported. Recent researches have shown that pure Han purple (degree of purity 99.5%) is, surprisingly, not purple in its pure state, but dark blue. The purple shade of Han purple was suggested coming from the red impurity of cuprite, Cu_2O , formed in the heat process [10].

Optimization of chemical and physical properties of materials is a major issue of industrial and academic material science research. Soft-chemistry synthesis of inorganic pigments was still seldom reported so far. It is a fundamental challenge to develop the green-chemistry strategies with characteristics of low cost, environmentally friendliness, atom economy and high quality of target products. The mild hydrothermal method is an important green chemistry strategy, which shows the great advantages of one-step and high quality of products. It performs under relatively high temperature and autogenic pressure, which change the solubility of reactants and facilitate specific reactions [20,21]. Hydrothermal method has been used to synthesize numerous functional materials like zeolites, nano-materials, and complex oxides [22–24].

We are interested in the study of multifunctional materials containing spin = 1/2 transition metals [25]. In this paper, we report the hydrothermal synthesis and properties of Chinese purple $\text{BaCuSi}_2\text{O}_6$ and dark blue $\text{BaCu}_2\text{Si}_2\text{O}_7$. A facile hydrothermal method was developed to synthesize these powder samples with good yield and purity, which is also a suitable method for industrial applications. The samples were selectively synthesized by mild hydrothermal treatment using the same reactants with stoichiometric ratios at 240 °C in a narrow range of pH values. Quantitative luminescence study confirms that $\text{BaCuSi}_2\text{O}_6$ exhibits NIR photoluminescence emission as similar as $\text{ACuSi}_4\text{O}_{10}$ ($A = \text{Ca}, \text{Sr}, \text{Ba}$) does. The magnetic properties of the samples are quantitatively analyzed, which is helpful in understanding the low dimensional magnetic systems.

2. Experimental

2.1. Synthesis

Reagent grade chemicals were used as received.

Purple polycrystalline powders of $\text{BaCuSi}_2\text{O}_6$ were synthesized by mild hydrothermal method. $\text{BaCl}_2 \cdot 4\text{H}_2\text{O}$ (0.244 g, 1 mmol), $\text{Na}_2\text{SiO}_3 \cdot 9\text{H}_2\text{O}$ (0.568 g, 2 mmol) and CuO (0.08 g, 1 mmol) powders as starting materials were mixed in distilled water (20 mL). The pH value of the solution was adjusted to 11 using HCl aqueous solution (2 mol/L), and then the mixture was sealed in autoclave with a Teflon liner (25 mL). The autoclave was heated up to 250 °C and kept it for 48 h, followed by cooling to room temperature by switching off the furnace. After the reaction the final pH value of the solution is 11.5. The product was treated by ultrasonic and the purple powders were further added into the NH_4Cl saturated solution in autoclave at 60 °C for 24 h, washing with distilled water and drying in air. The yield of the final collected products is 80%.

Dark blue polycrystalline powders of $\text{BaCu}_2\text{Si}_2\text{O}_7$ were synthesized by a mild hydrothermal method without further adjust of the pH value. $\text{BaCl}_2 \cdot 4\text{H}_2\text{O}$ (0.244 g, 1 mmol), $\text{Na}_2\text{SiO}_3 \cdot 9\text{H}_2\text{O}$ (0.568 g, 2 mmol) and 0.16 g CuO (0.16 g, 2 mmol) powders as starting materials were mixed in distilled water (20 mL). The pH value of the solution was 12. The mixture was sealed in autoclave with a Teflon liner (25 mL), then heated up to 250 °C and kept it for 48 h, followed by cooling to room temperature by switching off the furnace. Dark blue powders were obtained as a single phase after washing with distilled water and drying in air. The yield is 99%.

The energy dispersive spectroscopy (EDS) result (Fig. S4 in the Supporting Information) confirmed the composition of the products.

2.2. Properties

Ground powders of the products were used for powder X-ray measurement, infrared spectroscopy (KBr-pellets) measurement. The powder XRD patterns of products were collected on a PANalytical Empyrean diffractometer with $\text{Cu K}\alpha$ radiation ($\lambda = 0.15418$ nm) of 40 KV and 40 mA at room temperature by step scanning in an angle range of $10^\circ \leq 2\theta \leq 90^\circ$ and increments of 0.0263° were employed. Lattice constants were derived from Rietveld fits using the program package FULLPROF [26]. Scanning electron microscope (SEM) and EDS were performed using FIB-SEM instrument (a Helios NanoLab 600i Dual Beam System, FEI Company, with an EDS equipment (EDAX) from Ametek Company). The emission and excitation spectra of the phosphors were recorded using an Edinburgh Instruments FLS 920 spectrofluorimeter equipped with a continuous 450 W xenon lamp and using a R928 photomultiplier tube at 193 K detector coupled with a BaSO_4 coated integrating sphere. The magnetic properties were investigated with a MPMS (SQUID) VSM. X-ray photoemission spectroscopy (XPS, Thermo ESCALAB250) experiment was performed using monochromatic $\text{Al K}\alpha$ radiation (1486.6 eV), which was shown in the supporting information.

3. Results and discussion

3.1. Structure

The XRD patterns demonstrated that the hydrothermally synthetic $\text{BaCuSi}_2\text{O}_6$ and $\text{BaCu}_2\text{Si}_2\text{O}_7$ were single-phase. The XRD diagrams of $\text{BaCuSi}_2\text{O}_6$ and $\text{BaCu}_2\text{Si}_2\text{O}_7$ including the raw data plots, the global fitted profile, and the difference are shown in Fig. 1a and b. The refined values of unit cell parameters and main aspects of the structural features are summarized in Table 1. Examinations have

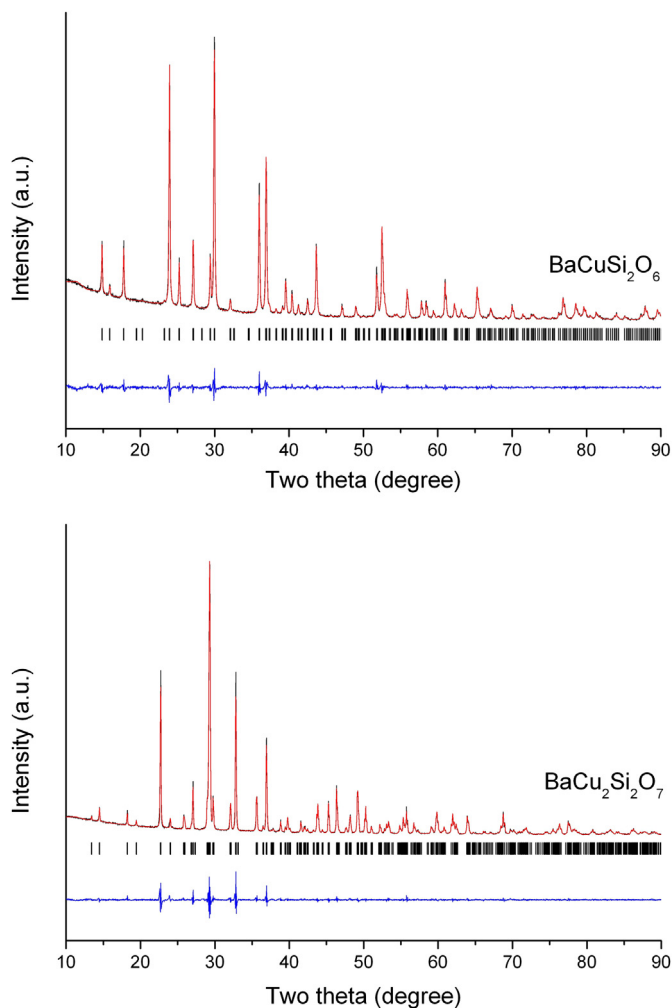


Fig. 1. The XRD patterns of the hydrothermally synthetic products $\text{BaCuSi}_2\text{O}_6$ and $\text{BaCu}_2\text{Si}_2\text{O}_7$.

shown that the crystal structure of $\text{BaCuSi}_2\text{O}_6$ undergoes a phase transition from the high-temperature phase with space group $I4/mmm$ to the room-temperature phase with a space group $I4_1/acd$ at ~ 610 K. Furthermore, the room-temperature phase transforms to low-temperature phase with space group $Ibam$ at ~ 107 K [19]. For hydrothermally prepared $\text{BaCuSi}_2\text{O}_6$, the observed room temperature powder X-ray diffraction data were Rietveld refined on the basis of a tetragonal structure with space group $I4_1/acd$ (reference structure ICSD No. 59964). In the structure of $\text{BaCuSi}_2\text{O}_6$, the copper silicate $\text{Cu}_2(\text{SiO}_3)_4$ layers are separated by the intermediate layers composed of Ba ions, which are parallel to the (001) crystallographic plane. Its basic building units are isolated $\text{Si}_4\text{O}_{12}^{8-}$ four-ring units in the layered framework, whose terminal oxygen atoms bind copper ions in a square-planar environment [10]. It results in the formation of an arrangement of Cu–Cu metal bond dimers (interatomic distance of 2.7473(44) Å in rows. The Cu–Cu dimers are well separated from each other with interdimer Cu–Cu distance of 4.9900(2) Å in the layers and Cu–Cu distances of 4.5217(28) Å between the dimers in adjacent layers.

For hydrothermally synthetic $\text{BaCu}_2\text{Si}_2\text{O}_7$, the observed powder X-ray diffraction data were Rietveld refined on the basis of an orthorhombic crystal structure with space group $Pnma$ (reference structure ICSD No. 68495). $\text{BaCu}_2\text{Si}_2\text{O}_7$ consist of a BaO_7 capped trigonal prism, CuO_4 tetrahedra and Si_2O_7 corner-sharing double-tetrahedral anions. Important structural feature is chains of the

Table 1

The refined values of unit cell parameters and main aspects of the structural features.

BaCuSi ₂ O ₆ lattice parameters at T = 298 K				
a, Å	9.97511(17)			χ^2 3.05
b, Å	9.97511(17)			R_{Bragg} 2.59
c, Å	22.2887(5)			RF factor 1.95
V, Å ³	2217.79(7)			R_p : 12.8, R_{wp} : 10.8, R_{exp} : 6.19
Space group	$I4_1/a c d$			
Atom	x	y	z	B_{iso} , Å ²
Ba	0.25	0.9902(4)	0.5	0.05(14)
Cu	0	0.25	0.06309(12)	0.06(14)
Si	0.2776(5)	0.7525(15)	0.876(3)	0.05(14)
O1	0.207(2)	0.721(3)	0.8164(14)	0.09(14)
O2	0.374(2)	0.876(2)	0.8607(7)	0.06(14)
O3	0.3164(20)	0.7803(19)	0.0645(11)	0.02(14)
BaCu ₂ Si ₂ O ₇ lattice parameters at T = 298 K				
a, Å	6.86317(15)			χ^2 5.74
b, Å	13.1773(3)			R_{Bragg} 3.798
c, Å	6.86317(15)			RF factor 2.392
V, Å ³	623.68(2)			R_p : 13.1, R_{wp} : 12.2, R_{exp} : 5.09
Space group	$P n m a$			
Atom	x	y	z	B_{iso} , Å ²
Ba	−0.0133(4)	0.25	0.9565(3)	0.02(15)
Cu	0.2208(6)	0.0034(4)	0.7919(5)	0.02(15)
Si	−0.0027(15)	0.1357(4)	0.4727(11)	0.03(15)
O1	0.097(2)	0.25	0.485(2)	0.01(15)
O2	−0.183(2)	0.1344(12)	0.6283(19)	0.02(15)
O3	−0.070(2)	0.1092(12)	0.2363(17)	0.02(15)
O4	0.1650(18)	0.0632(10)	0.531(2)	0.04(15)

corner-sharing CuO_4 tetrahedra along the c-axis and isolated Si_2O_7 corner-sharing double-tetrahedral units [10]. The intrachain Cu···Cu distance is 3.4725(49) Å and the nearest-neighbor inter-chain Cu···Cu distance is 3.4799(58) Å.

3.2. SEM

Digital photographs and SEM images of the samples are shown in Fig. 2a and b. It needs to be mentioned that digital photograph of hydrothermally synthetic $\text{BaCuSi}_2\text{O}_6$ shows that the sample is purple instead of the reported dark blue and no Cu_2O phase was detected in the products through XRD analysis. The SEM image of $\text{BaCuSi}_2\text{O}_6$ indicates the presence of homogeneous, well-shaped crystals with sizes of about 20 μm . The crystal forms are cornertruncated tetragonal pyramids with/without prism as shown in Fig. S3 (supporting information). The crystal faces are {111}, {001}, {100}, and prism face {110}. The sample consisted of nearly monodispersed particles and the particles were uniform in size and shape. Fig. 2b shows that dark blue $\text{BaCu}_2\text{Si}_2\text{O}_7$ is aggregated polycrystalline powder.

3.3. Synthesis

The powder samples of $\text{BaCuSi}_2\text{O}_6$ and $\text{BaCu}_2\text{Si}_2\text{O}_7$ were normally prepared through high temperature solid state reaction at 900 °C–1000 °C. The operational process is complicated and has high energy consumption. Moreover, it is quite hard to prepare the pure phase of the compounds since the impurities are always the by-products due to the complex phase diagram of BaO–CuO–SiO₂ system. Both single crystalline samples of $\text{BaCuSi}_2\text{O}_6$ and $\text{BaCu}_2\text{Si}_2\text{O}_7$ can be grown by the floating zone technique. But this method was limited by the special equipment, low yield and strict control. Hydrothermal synthesis of the compounds takes the advantage of soft-chemistry.

To determine the optimal reaction conditions for the formation of the products, the reactions were carried out at 220, 230, 240, and 250 °C for 6, 8, 10, 12, 24, 48 h, respectively. For atom economy, the molar ratio of reactants was fixed on the composition of the target

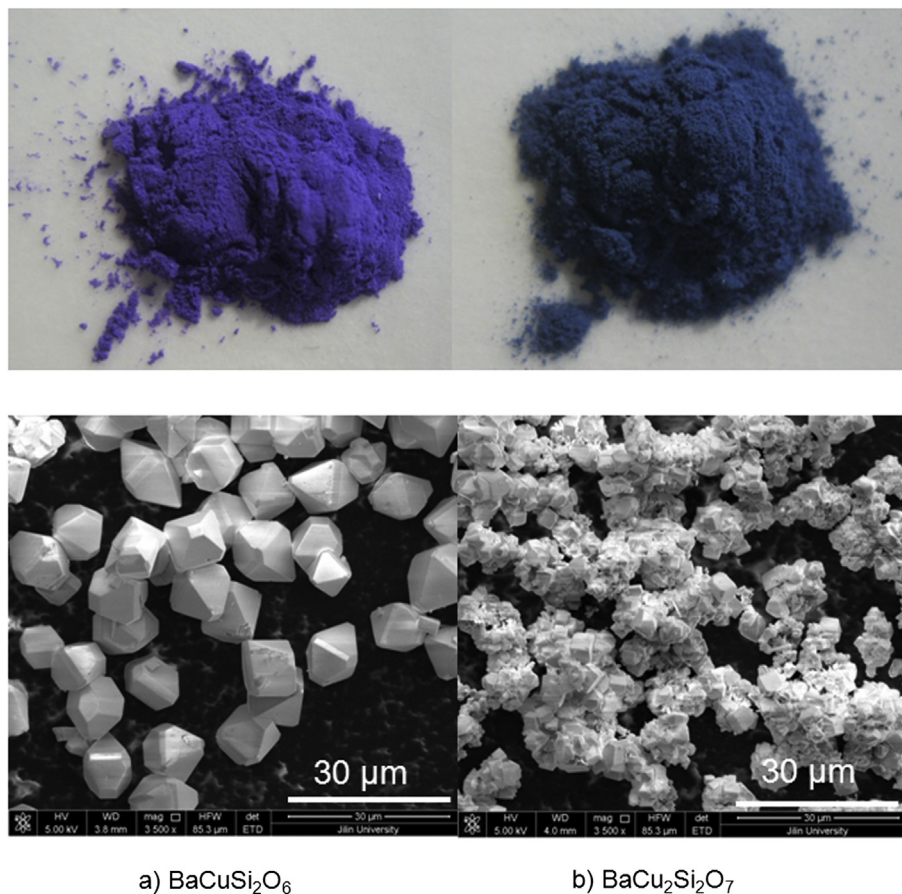
a) BaCuSi₂O₆b) BaCu₂Si₂O₇

Fig. 2. Top row is the digital photographs of Chinese purple (a) BaCuSi₂O₆ and dark blue (b) BaCu₂Si₂O₇. Bottom row show the SEM images of (a) BaCuSi₂O₆ and (b) BaCu₂Si₂O₇, respectively. (For interpretation of the references to color in this figure legend, the reader is referred to the web version of this article.)

compounds (BaO : CuO : 2SiO₂ for BaCuSi₂O₆ and BaO : 2CuO : 2SiO₂ for BaCu₂Si₂O₇). Experiments showed that a reaction temperature higher than 230 °C was quite necessary for all the samples. The reaction time longer than 12 h was preferred, although the target products can be detected with impurities (unreacted reactants) when the reaction time was 6 h. So we perform the hydrothermal treatments at 250 °C for 48 h for both compounds to study the influence of the pH value of the solution on the systems. The preparation of these two pigments is quite sensitive to the pH value of the basic solution. When the pH value of the solution is below 10, neither BaCuSi₂O₆ nor BaCu₂Si₂O₇ were detected in the final mixture powders. To successfully prepare crystalline BaCuSi₂O₆ powders, BaCl₂ solution was first mixed with Na₂SiO₃ solution, then CuO powders were added, the PH value of the final mixture was adjusted by HCl aqueous solution (2 mol/L) in the range of 10.5–12. After the hydrothermal treatment, the collected powders were a mixture of main products BaCuSi₂O₆ with few BaSi₂O₅, BaCO₃ and CuO. The saturated NH₄Cl solution is found quite powerful to dissolve the BaSi₂O₅, BaCO₃ and CuO impurities in hydrothermal condition at 60 °C overnight. After the hydrothermal treatment, BaCuSi₂O₆ crystalline powder was obtained as pure phase. If the pH value increased above 12, the powders are the mixtures of BaCuSi₂O₆, BaCu₂Si₂O₇, BaSi₂O₅, BaCO₃ and CuO. BaCu₂Si₂O₇ is more chemical stable than BaCuSi₂O₆ and is hard to be dissolved. It means that the higher pH value favors the formation of BaCu₂Si₂O₇. The suitable pH value for preparation of BaCu₂Si₂O₇ is found to be in the range of 11–13. BaCu₂Si₂O₇ is prepared in quite high yield (99%) and in good purity by this method. But the highest yield of BaCuSi₂O₆ is 80%.

3.4. IR

Fig. 3 presents the FTIR spectra of BaCuSi₂O₆ and BaCu₂Si₂O₇, the intense bands at 564 cm⁻¹ for BaCuSi₂O₆ and 537 cm⁻¹ for BaCu₂Si₂O₇ are assigned to the Si–O asymmetric deformation ν₄ mode. The strong bands observed between 800 cm⁻¹–1100 cm⁻¹ are most probably associated with Si–O antisymmetric ν₁ and ν₃ stretching modes for BaCuSi₂O₆ and BaCu₂Si₂O₇. 644 cm⁻¹ for BaCuSi₂O₆ and 617 cm⁻¹ for BaCu₂Si₂O₇ are assigned to Cu–O symmetric stretching mode. 724 cm⁻¹ for BaCuSi₂O₆ and 676 cm⁻¹ for BaCu₂Si₂O₇ are assigned to Si–O symmetric stretching mode. The appearance of the vibrations of Si–O and Cu–O groups clearly suggests the formation of the copper silicates [27].

3.5. Luminescence property

The luminescence property of hydrothermally synthetic BaCuSi₂O₆ was quantitative studied at room temperature. Being similar to ACuSi₄O₁₀ (A = Ca, Sr, Ba), BaCuSi₂O₆ shows broad NIR emission excited by a red laser [12]. Fig. 4 shows the absorption spectrum, excitation (λ_{em} = 925 nm) spectrum, the emission (λ_{ex} = 585 nm) spectrum and the luminescence decay profile of the hydrothermally synthetic BaCuSi₂O₆. Absorption spectrum shows three different electronic transitions (²B_{1g} → ²B_{2g}, ²E_g and ²A_{1g}) attributable to the square-planar Cu²⁺ ions. The center of the emission spectrum is at λ_{max} = 925 nm and the luminescence decay is 6.4 μs. The reported λ_{max} of the emission spectrum of Han purple is 980 nm [12]. The shift of λ_{max} was attributed to the slightly different microstructure caused by different synthetic strategies. When

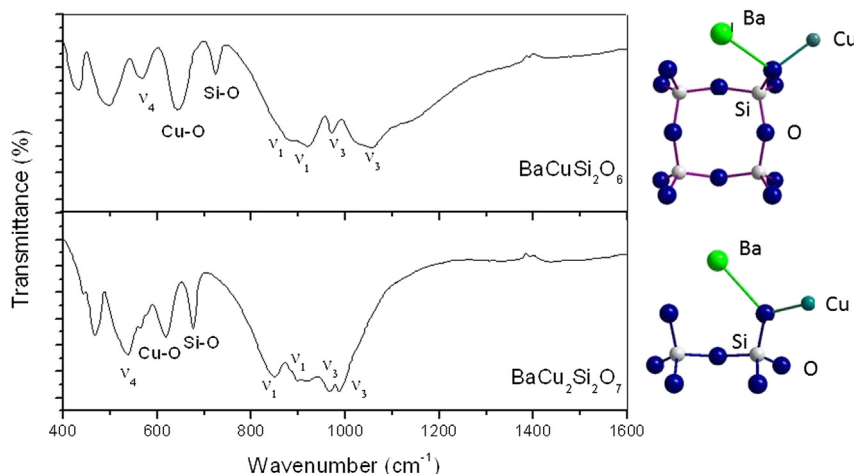


Fig. 3. FTIR spectra for $\text{BaCuSi}_2\text{O}_6$ and $\text{BaCu}_2\text{Si}_2\text{O}_7$. The structural features of the coordination around the silicate and the basic structural units are shown on right side.

irradiated by a red laser beam (optimal excitation wavelength, $\lambda_{\text{ex}} = 625$ nm), $\text{ACuSi}_4\text{O}_{10}$ ($A = \text{Ca}, \text{Sr}, \text{Ba}$) can effectively transform this light into fluorescent near-infrared (NIR) light in the 800–1200 nm range ($\lambda_{\text{max}} = 909$ nm for $\text{CaCuSi}_4\text{O}_{10}$, $\lambda_{\text{max}} = 914$ nm for $\text{SrCuSi}_4\text{O}_{10}$ and $\lambda_{\text{max}} = 948$ nm for $\text{BaCuSi}_4\text{O}_{10}$) [9]. The excitation bands in the visible region are very similar for all phosphors, an obvious shift of the ${}^2\text{B}_{1g} \rightarrow {}^2\text{A}_{1g}$ band is observed on going from $\text{CaCuSi}_4\text{O}_{10}$ to $\text{BaCuSi}_4\text{O}_{10}$. The emission quantum efficiencies of $\text{ACuSi}_4\text{O}_{10}$ ($A = \text{Ca}, \text{Sr}, \text{Ba}$) are pretty high (ca. 10%), but the hydrothermally prepared $\text{BaCuSi}_2\text{O}_6$ exhibits a low emission quantum efficiency in the near-infrared region ($\lambda_{\text{max}} = 925$ nm, $\Phi_{\text{EM}} = 0.9\%$). One consideration for this phenomenon is the influence of the Cu–Cu bonds in the structure of $\text{BaCuSi}_2\text{O}_6$ on the luminescence property. $\text{BaCu}_2\text{Si}_2\text{O}_7$ does not show luminescence in the visible and near-infrared spectral region at room temperature.

3.6. Magnetic property

The temperature dependence of the static magnetic susceptibility of $\text{BaCuSi}_2\text{O}_6$ was recorded between 2 and 300 K. No noticeable difference was found between ZFC and FC curves, which means there are no canted AFM, spin glass, and ferromagnetic (FM) indications. Fig. 5a presents the plots of experimental and calculated $\chi_{\text{mol}} - T$ under a 1 T field. As the temperature is lowered the

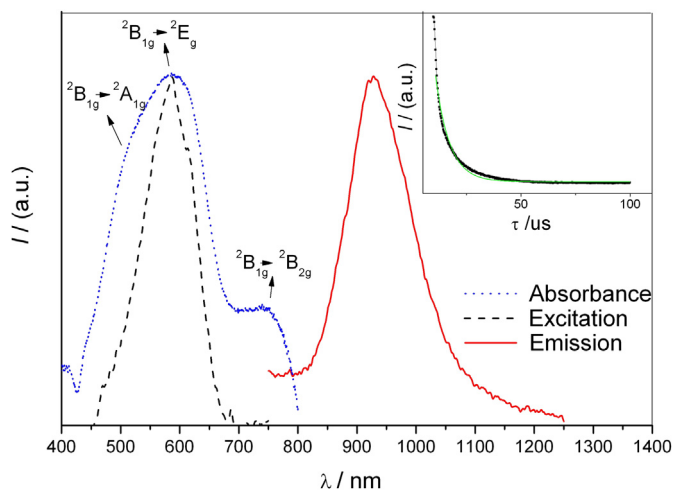


Fig. 4. Absorbance (dotted line), excitation (dashed line, $\lambda_{\text{em}} = 925$ nm) and emission (solid line, $\lambda_{\text{exc}} = 585$ nm) spectra of hydrothermally synthetic $\text{BaCuSi}_2\text{O}_6$. Inset: luminescence decay (6.4 μs , $\lambda_{\text{exc}} = 585$ nm).

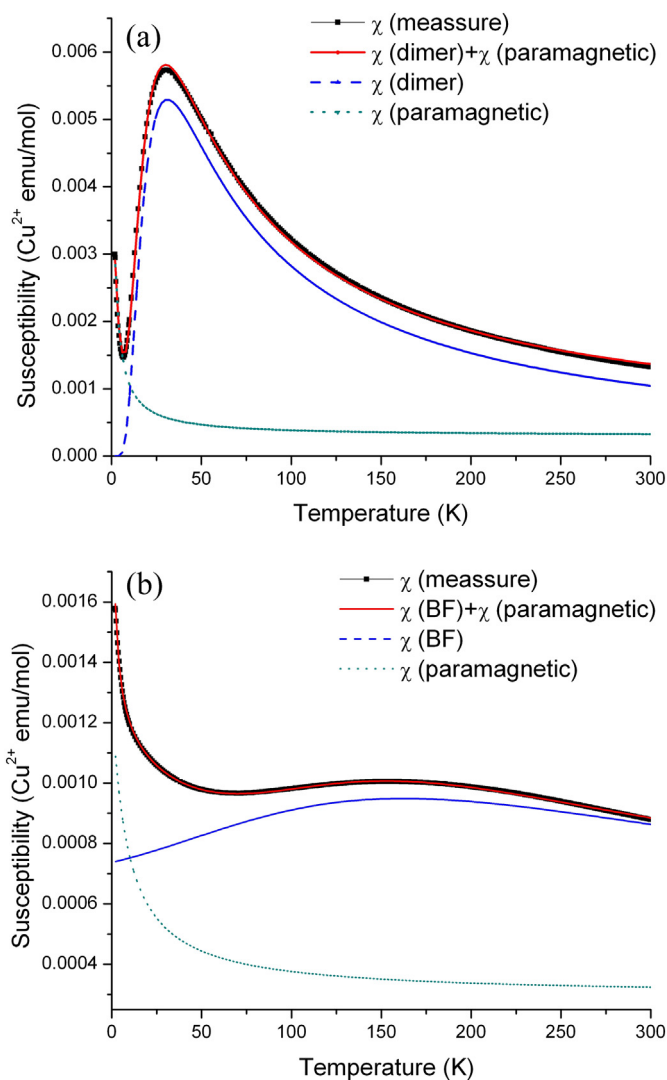


Fig. 5. Experimental and calculated χ_{mol} against temperature for $\text{BaCuSi}_2\text{O}_6$ (a) and $\text{BaCu}_2\text{Si}_2\text{O}_7$ (b): solid square for experiment data, red line for fitting data, dashed blue line for $\chi_{\text{spin}}(T)$ fitting data and dotted green line for paramagnetic contribution. (For interpretation of the references to color in this figure legend, the reader is referred to the web version of this article.)

susceptibility increases up to a maximum of $0.0057 \text{ emu mol}^{-1}$, which is reached at 30 K and then rapidly decreases to $0.0015 \text{ emu mol}^{-1}$ at 6.5 K. This behavior is characteristic of short ranged AFM interactions, which consistent with the reported SG AFM property of $\text{BaCuSi}_2\text{O}_6$. Below 6.5 K, a sharp increase in the form of “Curie-tail” occurs, which originates from paramagnetic impurities or defects. The high-temperature part of the susceptibility curve above 30 K was fitted by a Curie–Weiss expression $\chi = \chi_0 + C/(T - \theta_{\text{CW}})$. Where the temperature-independent term χ_0 accounts for the temperature independent diamagnetic and Van Vleck contributions, C is the curie constant, and θ_{CW} is the Curie–Weiss temperature. The best fitting result gives $\chi_0 = -4.8 \times 10^{-5} \text{ emu mol}^{-1}$, $C = 0.46 \text{ emu K mol}^{-1}$ and $\theta_{\text{CW}} = -41.7 \text{ K}$. The C value corresponds to the experimental effective magnetic moment of $1.91 \mu_{\text{B}}$, which is slight higher than the theoretical spin-only value of $1.73 \mu_{\text{B}}$ for Cu^{2+} due to the spin-orbital coupling effect. The negative Weiss constant suggests the dominant AFM interaction between Cu^{2+} cations. The SG behavior is predicted from several spin structure models, among which the dimer model are suitable for $\text{BaCuSi}_2\text{O}_6$ based on the Cu–Cu dimer crystal structure. In the whole range of temperatures, the $\chi_{\text{Cu-mol}}(T)$ data can be fitted with equation (1) using the spin–spin Hamiltonian in the form of $\hat{H} = J_{\text{intra}} \sum \hat{S}_i \hat{S}_{i+1}$:

$$\chi_{\text{Cu-mol}}(T) = \chi_0 + (1-x) \times C_{\text{imp}}/(T - \theta_{\text{imp}}) + x \times \chi_{\text{spin}}(T) \quad (1)$$

where the $C_{\text{imp}}/(T - \theta_{\text{imp}})$ is contribution of the magnetic impurity with x representing the mole fraction of the impurity. χ_0 is the temperature independent term from Van Vleck and diamagnetic contribution, the $\chi_{\text{dimer}}(T)$ is the spin-dimer model term [28]:

$$\chi_{\text{spin}}(T) = \frac{Ng^2\mu_{\text{B}}^2}{k_{\text{B}}T} \frac{2 \exp(-J/k_{\text{B}}T)}{1 + 3 \exp(-J/k_{\text{B}}T)} \quad (2)$$

where J is the effective intra-dimer coupling between two Cu^{2+} ions in the dimers. As shown in Fig. 5a, this dimer model provides a good fit yielding $J = -34.6 \text{ cm}^{-1}$, $g = 1.99$, $\chi_0 = 3.07 \times 10^{-4} \text{ emu (Cu}^{2+}\text{-mol)}^{-1}$, $C_{\text{imp}} = 0.015 \text{ emu K (Cu}^{2+}\text{-mol)}^{-1}$, $x = 0.43$, and $\theta_{\text{imp}} = -1.33 \text{ K}$ with $R^2 = 0.9992$. This result shows the strong paramagnetic contribution due to impurities or defects.

No noticeable difference was found between ZFC and FC curves of $\text{BaCu}_2\text{Si}_2\text{O}_7$ recorded between 2 and 300 K. Fig. 5b presents the plots of experimental and fitted $\chi_{\text{mol}} - T$ under a 1 T field. The broad maximum in $\chi_{\text{mol}} - T$ at around 150 K is a typical feature of a low-dimensional magnetic system. A sharp “Curie-tail” occurs below 50 K, which originates from the paramagnetic contribution. To determine the dominant AFM exchange parameter J , the magnetic susceptibility was fitted with the expression (1). The $\chi_{\text{spin}}(T)$ is the contribution of the spin $S = 1/2$ Heisenberg antiferromagnetic chains [29]. We took the isotropic one-dimensional $S = 1/2$ model of Bonner and Fisher [30,31]:

$$\chi_{\text{spin}}(T) = \frac{Ng^2\mu_{\text{B}}^2}{k_{\text{B}}T} \frac{0.25 + 0.074975(-J/k_{\text{B}}T) + 0.075236(-J/k_{\text{B}}T)^2}{1 + 0.9931(-J/k_{\text{B}}T) + 0.172135(-J/k_{\text{B}}T)^2 + 0.757825(-J/k_{\text{B}}T)^3} \quad (3)$$

As shown in Fig. 5b, the best fit yields $J = -173.3 \text{ cm}^{-1}$, $g = 1.90$, $\chi_0 = 2.96 \times 10^{-4} \text{ emu (Cu}^{2+}\text{-mol)}^{-1}$, $C_{\text{imp}} = 0.049 \text{ emu K (Cu}^{2+}\text{-mol)}^{-1}$, $x = 0.18$, and $\theta_{\text{imp}} = -8.93 \text{ K}$ with $R^2 = 0.990$. The magnetic property of $\text{BaCu}_2\text{Si}_2\text{O}_7$ is consistent with the quasi-one-dimensional Cu^{2+} chain structure of $\text{BaCu}_2\text{Si}_2\text{O}_7$.

4. Conclusion

Chinese purple $\text{BaCuSi}_2\text{O}_6$ and dark blue $\text{BaCu}_2\text{Si}_2\text{O}_7$ are synthesized by a mild hydrothermal method under a narrow pH range at $250 \text{ }^\circ\text{C}$. This soft-chemistry method is available for industrial applications and has the characteristics of ease of handling, green chemistry, and high quality of products. It makes Chinese purple $\text{BaCuSi}_2\text{O}_6$ and dark blue $\text{BaCu}_2\text{Si}_2\text{O}_7$ easily obtained pigments. The Chinese purple $\text{BaCuSi}_2\text{O}_6$ shows novel NIR emission irradiated by a visible light, which means the ancient pigment is also a functional phosphor. $\text{BaCuSi}_2\text{O}_6$ shows spin gapped antiferromagnetic property and dark blue $\text{BaCu}_2\text{Si}_2\text{O}_7$ exhibits quasi-one-dimensional antiferromagnetic property. Future study will focus on the development of the soft-chemistry strategy for functional inorganic pigments.

Acknowledgments

This work was supported by the National Natural Science Foundation of China (Grants 21301067, 21131002).

Appendix A. Supplementary data

Supplementary data related to this article can be found at <http://dx.doi.org/10.1016/j.dyepig.2014.01.017>.

References

- [1] Warner TE. Synthesis, properties and mineralogy of important inorganic materials. Hoboken, NJ: Wiley; 2011.
- [2] Berke H. Chemistry in ancient times: the development of blue and purple pigments. *Angew Chem Int Ed* 2002;41:2483–7.
- [3] Accorsi G, Verri G, Bolognesi M, Armaroli N, Clementi C, Miliani C, et al. The exceptional near-infrared luminescence properties of cuprorivaite (Egyptian blue). *Chem Commun* 2009;23:3392–4.
- [4] Wiedemann HG. Thermoanalytische untersuchung von baumaterialien ägyptischer mumien-särge. *J Therm Anal* 1998;52:93–107.
- [5] Wiedemann HG, Bayer G, Reller A. Egyptian blue and Chinese blue – production technologies and applications of two historically important blue pigments. In: *Actes de la Table Ronde: Ravello, Edipuglia, Bari, Italy; 1997*. pp. 195–203.
- [6] Kendrick E, Kirk CJ, Dann SE. Structure and colour properties in the Egyptian blue family, $\text{M}_{1-x}\text{M}'_x\text{CuSi}_4\text{O}_{10}$, as a function of M, M' where M, M' = Ca, Sr and Ba. *Dyes Pigments* 2007;73:13–8.
- [7] Jose S, Reddy ML. Lanthanumstrontium copper silicates as intense blue inorganic pigments with high near-infrared reflectance. *Dyes Pigments* 2013;98:540–6.
- [8] McDaniel DJ, Barrett CA, Sharafi A, Salguero TT. Nanoscience of an ancient pigment. *J Am Chem Soc* 2013;135:1677–9.
- [9] Borisov SM, Würth C, Genger UR, Klimant I. New life of ancient Pigments: application in high-performance optical sensing materials. *Anal Chem* 2013;85:9371–7.
- [10] Berke H. The invention of blue and purple pigments in ancient times. *Chem Soc Rev* 2007;36:15–30.
- [11] Yang HX, Downs RT, Evans SH, Pinch WW. Scottyite, the natural analog of synthetic $\text{BaCu}_2\text{Si}_2\text{O}_7$, a new mineral from the Wessels mine, Kalahari manganese fields, South Africa. *Am Mineral* 2013;98:478–84.
- [12] Pozza G, Ajò D, Chiari G, Zuane DF, Favaro M. Photoluminescence of the inorganic pigments Egyptian blue, Han blue and Han purple. *J Cult Herit* 2000;1:393–8.
- [13] Han A, Ye MQ, Zhao MC, Liao JJ, Wu TT. Crystal structure, chromatic and near-infrared reflective properties of iron doped YMnO_3 compounds as colored cool pigments. *Dyes Pigments* 2013;99:527–30.
- [14] George G, Vishnu VS, Reddy MLP. The synthesis, characterization and optical properties of silicon and praseodymium doped $\text{Y}_6\text{MoO}_{12}$ compounds: environmentally benign inorganic pigments with high NIR reflectance. *Dyes Pigments* 2011;88:109–15.
- [15] Giamarchi T, Rüegg C, Tchernyshyov O. Bose–Einstein condensation in magnetic insulators. *Nat Phys* 2008;4:198–204.

- [16] Jaime M, Correa VF, Harrison N, Batista CD, Kawashima N, Kazuma Y, et al. Magnetic-field-induced condensation of triplons in Han purple pigment $\text{BaCuSi}_2\text{O}_6$. *Phys Rev Lett* 2004;93: 087203: 1–4.
- [17] Sebastian SE, Harrison N, Batista CD, Balicas L, Jaime M, Sharma PA, et al. Dimensional reduction at a quantum critical point. *Nat (London)* 2006;441:617–20.
- [18] Zheludev A, Kenzelmann M, Raymond S, Ressouche E, Masuda T, Kakurai K, et al. Energy separation of single-particle and continuum states in an $S = 1/2$ weakly coupled chains antiferromagnet. *Phys Rev Lett* 2000;85:4799–802.
- [19] Sheptyakov DV, Pomjakushin VY, Stern R, Heinmaa I, Nakamura H, Kimura T. Two types of adjacent dimer layers in the low-temperature phase of $\text{BaCuSi}_2\text{O}_6$. *Phys Rev B* 2012;86: 014433:1–8.
- [20] Stampfer ES, Sheets WC, Bertoni MI, Prellier W, Mason TO, Poeppelmeier KR. Temperature driven reactant solubilization synthesis of BiCuOSe . *Inorg Chem* 2008;47:10009–16.
- [21] Sheets WC, Mugnier E, Barnabé A, Marks TJ, Poeppelmeier KR. Hydrothermal synthesis of delafossite-type oxides. *Chem Mater* 2006;18:7–20.
- [22] Wang XQ, Liu LM, Jacobson AJ. Nanoporous copper silicates with one-dimensional 12-ring channel systems. *Angew Chem Int Ed* 2003;42:2044–7.
- [23] Wang X, Zhuang J, Peng Q, Li YD. A general strategy for nanocrystal synthesis. *Nat* 2005;437:121–4.
- [24] Chang HY, Kim SH, Halasyamani PS, Ok KM. Alignment of lone pairs in a new polar material: synthesis, characterization, and functional properties of $\text{Li}_2\text{Ti}(\text{IO}_3)_6$. *J Am Chem Soc* 2009;131:2426–7.
- [25] Chen Y, Liu T, He C, Duan CY. Mild hydrothermal synthesis, structure and characterization of the vanadyl phosphate hydrate $\text{Pb}(\text{VOPO}_4)_2 \cdot 3\text{H}_2\text{O}$: the formation of spin dimers in a three dimensional crystal structure. *J Mater Chem* 2012;22:19872–81.
- [26] Rodriguez-Carvajal J. FULLPROF2000. Version 3.30, June 2005. Gif-sur-Yvette, Cedex, France: Laboratoire Léon Brillouin CEA-CNRS; 2005., <http://www.ill.eu/sites/fullprof/>.
- [27] Nakamoto K. In *Infrared and Raman spectra of inorganic and coordination compounds*. 3rd ed. New York: Wiley-Interscience, John Wiley & Sons, Inc; 1978.
- [28] Yahia HB, Gaudin E, Darriet J, Dai DD, Whangbo MH. Comparison of the crystal structures and magnetic properties of the low- and high-temperature forms of AgCuPO_4 : crystal structure determination, magnetic susceptibility measurements, and spin dimer analysis. *Inorg Chem* 2006;45:5501–9.
- [29] Johnston DC, Kremer RK, Troyer M, Wang X, Klümper A, Bud'ko SL, et al. Thermodynamics of spin $S = 1/2$ antiferromagnetic uniform and alternating-exchange Heisenberg chains. *Phys Rev B* 2000;61:9558–606.
- [30] Bonner JC, Fisher ME. Linear magnetic chains with anisotropic coupling. *Phys Rev* 1964;135:A640–58.
- [31] Möller A, Schmitt M, Schnelle W, Förster T, Rosner H. AgCuVO_4 : a quasi-one-dimensional $S = 1/2$ chain compound. *Phys Rev B* 2009;80: 125106:1–8.